A&A 473, 545–550 (2007)
DOI: 10.1051/0004-6361:20077508

Astronomy & Astrophysics

Exploring the connection between the stellar wind and the non-thermal emission in LS 5039⋆,⋆⋆

V. Bosch-Ramon[1], C. Motch[2], M. Ribó[3], R. Lopes de Oliveira[2,4], E. Janot-Pacheco[4], I. Negueruela[5], J. M. Paredes[3], and A. Martocchia[6]

[1] Max Planck Institut für Kernphysik, Saupfercheckweg 1, Heidelberg 69117, Germany
e-mail: vbosch@mpi-hd.mpg.de
[2] Observatoire Astronomique, rue de l'Université 11, 67000 Strasbourg, France
e-mail: motch@astro.u-strasbg.fr
[3] Departament d'Astronomia i Meteorologia, Universitat de Barcelona, c/Martí i Franquès 1, 08028 Barcelona, Catalonia, Spain
e-mail: mribo@am.ub.es; jmparedes@ub.edu
[4] Universidade de São Paulo, Instituto de Astronomia, Geofísica e Ciências Atmosféricas – IAG, Departamento de Astronomia, Rua do Matão 1226, 05508-900 São Paulo, Brazil
e-mail: [rlopes;janot]@astro.iag.usp.br
[5] Dpto. de Física, Ingeniería de Sistemas y Teoría de la Señal, Universidad de Alicante, Apdo. 99, 03080 Alicante, Spain
e-mail: ignacio@dfists.ua.es
[6] Istituto Nazionale di Astrofisica, via del Fosso del Cavaliere 100, 00133 Roma, Italy
e-mail: andrea.martocchia@iasf-roma.inaf.it

Received 19 March 2007 / Accepted 10 July 2007

ABSTRACT

Context. LS 5039 has been observed with several X-ray instruments so far showing quite steady emission in the long term and no signatures of accretion disk. The source also presents X-ray variability at orbital timescales in flux and photon index. The system harbors an O-type main sequence star with moderate mass-loss. At present, the link between the X-rays and the stellar wind is unclear.
Aims. We study the X-ray fluxes, spectra, and absorption properties of LS 5039 at apastron and periastron passages during an epoch of enhanced stellar mass-loss, and the long term evolution of the latter in connection with the X-ray fluxes.
Methods. New *XMM-Newton* observations were performed around periastron and apastron passages in September 2005, when the stellar wind activity was apparently higher. April 2005 *Chandra* observations on LS 5039 were revisited. Moreover, a compilation of Hα *EW* data obtained since 1992, from which the stellar mass-loss evolution can be approximately inferred, was carried out.
Results. *XMM-Newton* observations show higher and harder emission around apastron than around periastron. No signatures of thermal emission or a reflection iron line indicating the presence of an accretion disk are found in the spectrum, and the hydrogen column density ($N_{\rm H}$) is compatible with being the same in both observations and consistent with the interstellar value. 2005 *Chandra* observations show a hard X-ray spectrum, and possibly high fluxes, although pileup effects preclude conclusive results from being obtained. The Hα *EW* shows yearly variations of ∼10%, and does not seem to be correlated with X-ray fluxes obtained at similar phases, unlike what is expected in the wind accretion scenario.
Conclusions. 2005 *XMM-Newton* and *Chandra* observations are consistent with 2003 *RXTE*/PCA results, namely moderate flux and spectral variability at different orbital phases. The constancy of the $N_{\rm H}$ seems to imply that either the X-ray emitter is located at $\gtrsim 10^{12}$ cm from the compact object, or the density in the system is 3 to 27 times smaller than that predicted by a spherical symmetric wind model. We suggest that the multiwavelength non-thermal emission of LS 5039 is related to the observed extended radio jets and is unlikely to be produced inside the binary system.

Key words. X-rays: binaries – stars: individual: LS 5039 – radiation mechanisms: non-thermal

1. Introduction

LS 5039 (V479 Sct) is an X-ray binary (Motch et al. 1997) located at 2.5 ± 0.5 kpc (Casares et al. 2005, C05 hereafter). The orbital ephemeris of the source was obtained by C05, being: T_0 = HJD 2 451 943.09 ± 0.1, periastron passage (phase 0.0); $P_{\rm orb}$ = 3.90603 ± 0.00017 days, orbital period; e = 0.35 ± 0.04, eccentricity; and i ∼ 15°–60°, inclination[1]. LS 5039 presents (∼1–100 milliarcsec) radio jets (Paredes et al. 2000, 2002), shows X-ray variability on timescales similar to the orbital one (Bosch-Ramon et al. 2005, BR05 hereafter), and has been detected at very high-energy gamma-rays

⋆ The Hα results presented here are based on observations made with ESO Telescopes at the La Silla or Paranal Observatories under program IDs 67.D-0229(A), 69.D-0628(A) and 075.D-0591(A); the Observatoire de Haute-Provence; the Observatório do Pico dos Dias / LNA, Brazil; the G. D. Cassini telescope operated at the Loiano Observatory by the Osservatorio Astronómico di Bologna; and the Nordic Optical Telescope, operated on the island of La Palma jointly by Denmark, Finland, Iceland, Norway, and Sweden, in the Spanish Observatorio del Roque de los Muchachos of the Instituto de Astrofisica de Canarias (those data were taken using ALFOSC, which is owned by the Instituto de Astrofísica de Andalucía (IAA) and operated at the Nordic Optical Telescope under agreement between IAA and the NBIfAFG of the Astronomical Observatory of Copenhagen).

⋆⋆ Table 2 is only available in electronic form at http://www.aanda.org

[1] We note that throughout this work, the errors in phases -not shown- range between 0.03–0.04 due to the uncertainties in T_0 and $P_{\rm orb}$.

(Aharonian et al. 2005), which virtually confirms its association with a *CGRO*/EGRET (EGRET from now on) source (Paredes et al. 2000). Interestingly, the TeV emission varies with the orbital period (Aharonian et al. 2006). Recently, LS 5039 has also been detected by *INTEGRAL* (Goldoni et al. 2006) up to 100 keV (De Rosa et al. 2006). The nature of the compact object is still uncertain. C05 suggest that it may be a black hole, although there is an ongoing debate on this issue, and some authors have proposed that LS 5039 is in fact a young non-accreting pulsar (e.g., Martocchia et al. 2005 – M05 hereafter; Dubus 2006).

All X-ray observations performed to date by imaging instruments have failed to show strong flux and photon index variations. *RXTE*/PCA (*RXTE*) also observed the source in 1998 (Ribó et al. 1999) and 2003 (BR05), although the latter authors found that *RXTE* data were likely contaminated by diffuse X-rays from the Galactic Ridge. Nonetheless, 2003 *RXTE* data showed orbital flux variations by a factor of ∼2 unrelated to diffuse background emission, peaking smoothly around phase 0.8 and more sharply at other phases. These peaks were apparently accompanied by spectral hardening. At phases ∼0.8, higher and harder emission has been also observed at TeV energies (Aharonian et al. 2006), and simultaneous *Chandra* observations have apparently shown similar behavior in X-rays (Horns et al. 2006). A possible relationship between the mass-loss rate of the companion star and the X-ray emission in LS 5039 was discussed in previous studies and a correlation suggested in the context of wind accretion powering the X-rays (e.g., Reig et al. 2003 – R03 hereafter; McSwain et al. 2004 – MS04 hereafter).

We present here recent *XMM-Newton* observations of LS 5039 carried out in September 2005 during periastron and apastron passages, in an epoch of inferred high stellar mass-loss rate. *Chandra* data taken in the same year are reanalyzed. In addition, we investigate the long-term Hα *EW* evolution, linked to the evolution of the stellar mass-loss rate, and compare it with the X-ray fluxes looking for possible correlations. These results are put in context with information at other wavelengths and a physical scenario is suggested.

2. X-ray observations

2.1. *XMM-Newton* observations

The *XMM-Newton* observations presented here were performed in two runs, on the 22th and 24th of September 2005, with EPIC pn on times of 15.8 ks and 10.4 ks (very similar to those of MOS1 and MOS2), respectively (Table 1). The corresponding observed phases are 0.49–0.53, around apastron, and 0.02–0.05, right after periastron. These observations were triggered in the context of a target of opportunity (ToO) program linked to the strength of the Hα line, which gives information on the state of the stellar wind. The Hα *EW* was found in late August 2005 to be above −2.4 Å, defined as the threshold set to trigger the *XMM-Newton* observations and significantly larger than the values observed during previous years. *XMM-Newton* observations were carried out in September due to visibility constraints. The physical motivation of the ToO was that, if direct accretion of the stellar wind is taking place in the system, the detection of higher X-ray fluxes, and/or accretion spectral features such as a multi-color black-body and/or a reflection iron line, seems more likely during epochs of larger stellar mass-loss, i.e. higher accretion rate. The convention for the Hα *EW* in this study is to take this value as negative when in absorption, i.e. it increases in the same sense as the stellar mass-loss rate.

Table 1. X-ray observations and spectral results.

Date	2005-04-13	2005-09-22	2005-09-24
Mission	*Chandra*	*XMM-Newton*	*XMM-Newton*
OBSID	6259	0202950201	0202950301
Orbital phase	0.86–0.87	0.49–0.53	0.02–0.05
MJD_{start}	53473.116	53635.714	53637.779
MJD_{stop}	53473.174	53635.897	53637.899
f_x (L_x)	2 ± 1 (1.5)	$1.18^{+0.03}_{-0.07}$ (0.9)	0.74 ± 0.07 (0.6)
Photon index	1.1 ± 0.2	1.51 ± 0.02	1.59 ± 0.03
N_H (*phabs*)	6 ± 1	6.3 ± 0.1	6.2 ± 0.2

Notes: fluxes and luminosities are given unabsorbed in the 0.3–10 keV energy band in units of 10^{-11} erg cm^{-2} s^{-1} and 10^{34} erg s^{-1}, respectively. The N_H units are 10^{21} cm^{-2}. Quoted errors are at the 1σ confidence level. Ephemeris taken from C05.

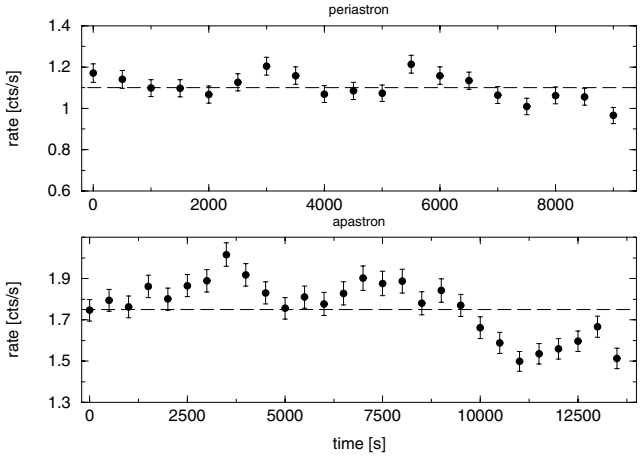

Fig. 1. Lightcurves at periastron (*top*) and apastron (*bottom*). The average value is given as a long-dashed line. The time axis is different for each lightcurve.

We focus here on the data obtained with the EPIC instrument, since the X-ray spectrometer (RGS) data had insufficient statistics because of the faintness of the source. The MOS and pn cameras were in small and full windows respectively, with medium filters. Reduction and analysis of the data were performed following the standard procedure using the SAS 7.0.0 software package to filter data and create spectra and lightcurves, and Xspec 12.3.0 for the spectral analysis. No large background flare was present in either of the two data sets. The 0.3–12 keV count rates per camera around phases 0.5 and 0.0 were 0.46 and 0.29 cts s^{-1} for MOS1, 0.47 and 0.30 cts s^{-1} for MOS2, and 1.09 and 0.71 cts s^{-1} for pn, respectively.

The lightcurves for the two runs, adding the data from pn, MOS1 and MOS2 cameras and taking time bins of 500 s, are presented in Fig. 1 for periastron (bottom) and apastron (top) passages, respectively. Around apastron, the emission is variable on timescales of a few hours. A constant fit to the data gives a reduced χ squared (χ^2_{red}; 27 degrees of freedom – d.o.f. –) of 6.8, and the maximum count rate variation is ≈25% during this run, with deviations of $\approx\pm5\sigma$ from the mean value. Around periastron, the lightcurve is still somewhat inconsistent with being constant (χ^2_{red} = 2.4; 18 d.o.f.), with a maximum count rate variation of ≈25% and deviations of $\approx\pm2\sigma$ from the mean value. We also studied the hardness ratio evolution for both runs, which is compatible with being constant. Searching for pulsations, no significant period peaks are found in the frequency range of 0.01 to 83 Hz and the pulsed fraction has been constrained to be

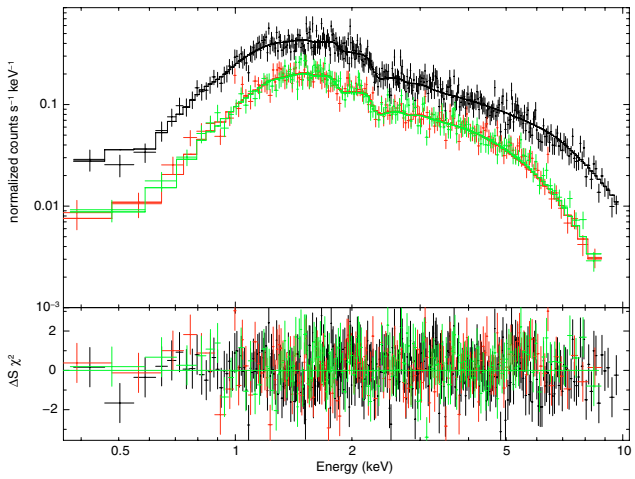

Fig. 2. Spectral data from pn (*upper spectrum*), MOS1 and MOS2 (*lower spectra*) cameras, and the best fit to the three of them: an absorbed power-law, around phase 0.5 (those around phase 0.0 look very similar and are not shown here). The deviations in σ of the model from the data are shown in the lower panel.

less than ≈10%, similar to the results reported by M05 for 2003 *XMM-Newton* data.

We show in Fig. 2 the spectrum of the source around phase 0.5, altogether with the deviations in σ of the best fit model from the data. We have added the data obtained from the pn, MOS1 and MOS2 cameras. The spectrum around phase 0.0 is not shown though it looks very similar to that around phase 0.5. The spectrum of the emission is well represented by an absorbed power-law ($\chi^2_{\rm red}$ = 1.08 –637 d.o.f. – and 0.93 – 312 d.o.f. – for phases 0.5 and 0.0, respectively). The unabsorbed fluxes, photon indices (0.3–10 keV) and $N_{\rm H}$ values for the two runs are given in Table 1. The flux between periastron and apastron increases by 60% at a level of 4.4σ, and the photon index rises up marginally by 0.08 (2.2σ). This behavior, despite being marginal, supports the *RXTE* finding that the higher the flux, the harder the spectrum. For the absorption model, we used *phabs*, which assumes updated photoelectric cross-sections from Balucinska-Church & Mc Cammon (1992). The $N_{\rm H}$ values are compatible within errors between both runs.

A multi-color black-body (*bbody*) and a Gaussian line component were added, separately, to the absorbed power-law model for the two runs. We obtain upper-limits for the multi-color black-body flux in the two runs (∼10% the total flux) similar to those found by M05. At the same phases, we looked for flux upper-limits of a possible iron line and obtain an upper-limit for the flux of about 2% of the total. The lack of a multi-color black-body and a line component in the data is consistent with previous imaging instrument observations and confirms that the iron line reported in Ribó et al. (1999) was due to background contamination.

2.2. Chandra data

In April 2005, *Chandra* observed LS 5039 in the ACIS-S mode (time frame: 1.6 s) during 5 ks (Table 1) at a time corresponding to the orbital phase 0.86–0.87, at which *RXTE* observed a smooth maximum (BR05). The *Chandra* Interactive Analysis of Observations software package (CIAO 3.3.0.1) was used to extract the spectrum and the lightcurve, following the standard procedure given in the *Chandra* analysis threads. *Sherpa* (CIAO 3.3) was used to analyze the spectrum. The ACIS count rate was relatively high, 0.3 cts s^{-1} (0.3–10 keV). *Chandra* data are likely to be moderately affected by pileup (see *The Chandra Proposers' Observatory Guide*, Fig. 6.19). Therefore, we used the pileup model available in Sherpa to obtain our fits (Davis 2001).

The spectrum can be well fitted by a power-law model with absorption (*xsphabs*, the sherpa version of *phabs*) and pileup. We perform the spectral fit fixing the event pileup fraction parameter to 0.95 to avoid unreasonably high values for the flux (i.e. $\sim 10^{-10}$ erg cm^{-2} s^{-1}). We obtain a relatively low grade migration parameter of 0.2 ± 0.1. The pileup fraction is ≈11%. Therefore, the effect of pileup on these observations seems to be only moderate. The results of our fit are given in Table 1. The photon index value, harder than that found in almost all previous observations, has also been calculated without a pileup model by removing the central pixels, i.e. the most affected by pileup (pileup effects can indeed produce an artificial hardening of the spectrum), obtaining compatible spectral results. No disk or line components are required to fit the data. The lightcurve is consistent with being constant.

3. Hα line observations

We present in Table 2 (presented only electronically on-line) the list of the journal of optical observations and the corresponding Hα *EW*. Most of these optical spectroscopic observations of LS 5039 were carried out by us at regular time intervals between September 2000 and July 2002, to construct an orbital solution and monitor the variations of the *EW* of the Hα line, the most convenient line to study the wind of LS 5039. A new observing campaign was initiated in 2004 to determine the time at which the Hα *EW* would go above −2.4 Å, the condition required to trigger the 2005 *XMM-Newton* observations.

Various instruments were used in the course of this extended campaign. At the Observatoire de Haute-Provence (OHP), we observed most of the time with the ELODIE Echelle Spectrometer. Some additional spectra were obtained with the CARELEC spectrograph (Lemaitre et al. 1990). At ESO, the majority of the data were acquired with the FEROS[2] Echelle Spectrometer (Kaufer et al. 1999). FORS1 observed the source on two occasions in 2001. LS 5039 was also monitored over an orbital cycle with the ESO-NTT and EMMI during a dedicated program in July 2002. Finally, the spectrum obtained in 1992 is described in Motch et al. (1997). The spectra obtained on 1999-08-18 and 2004-07-19 were acquired at Osservatorio Astronomico di Bologna with the 1.52 m Loiano telescope and the BFOSC instrument and at the NOT we used the ALFOSC spectrograph. At the Brazilian National Observatory of the Observatório do Pico dos Dias, we used the ESPCASS Cassegrain grating spectrometer mounted on either the 0.6 m or the 1.6 m telescope. Instrument settings are summarized in Table 2 (on-line).

The Hα line has an intrinsic *FWHM* of ∼8 Å and is therefore relatively well resolved in most of our observations. Due to the southern location of the object, observations from the OHP and Canary Islands were always acquired at a high air mass, typically 1.9 at OHP. At these high air masses, several telluric absorption lines start to be noticeable and can substantially change the value of the Hα *EW*, either by directly adding to the absorption profile or by changing the value of the reference continuum. These lines are clearly seen in the high resolution ELODIE

[2] All FEROS observations were obtained during the Brazilian time allocation.

individual spectra. In the $\lambda\lambda$ range 6540–6580 Å, the most important telluric lines are located at $\lambda\lambda$ 6543.89, 6546.61, 6552.62, 6557.16, 6564.19, 6572.06 and 6574.83 Å. Guided by the atmospheric transmission lines atlas of Hinkle et al. (2003), we could easily remove the sharp lines due to telluric absorption from the high resolution ELODIE spectra and thus fully correct for atmospheric effects. Some of the FEROS spectra also exhibited evidence of well resolved atmospheric lines at a much lower level than at OHP and could be removed as well.

At a resolution of ∼1000 or less, however, atmospheric lines are heavily smeared and cannot be simply removed. They appear as shoulders in the blue and red wings of the broad Hα absorption line of LS 5039 or as slight distortion in the central line profile. We estimated the effect of these lines on the measured equivalent widths by scaling the absorption spectrum of Hinkle et al. (2003) so that they could match the equivalent widths of the narrow lines observed in the mean OHP ELODIE spectrum and applying it to a Gaussian Hα line profile fitting that of LS 5039. Because of the low altitude and relatively high humidity level, the atmospheric effects at OHP are noticeably large. We find that telluric absorptions can easily add 0.4 Å to the equivalent width of a low resolution spectrum at airmass 1.9. Low resolution spectra obtained at OHP were thus rectified using continuum regions clear of known atmospheric lines and their *EW* were then corrected by 0.4 Å. In the absence of clear measurements or estimates of water vapor column we did not try to correct the other measurements obtained at lower air masses and under much dryer conditions.

4. Discussion

4.1. Evolution of the Hα EW and the X-rays

We have studied the available Hα data (this work; C05; MS04; R03) and found, as already suggested (e.g. McSwain & Gies 2002; R03), that the Hα *EW* is not compatible with being constant ($\chi^2_{\rm red}$ = 3.7; 96 d.o.f.), with a weighted mean value of -2.66 ± 0.01 Å, where the error has been computed using the error propagation method. All errors quoted here are 1σ. The weighted standard deviation of the sample is 0.21 Å, giving an idea of the dispersion degree of the individual points. The yearly averages with their corresponding standard deviations, altogether with the individual points, are shown in Fig. 3. For those years when only one measurement is available, we show just the individual point with its error. The yearly mean errors are typically 0.02–0.1 (not shown in the plot), being significantly smaller than the yearly standard deviations (shown in the plot), 0.04–0.29 Å. This relatively large dispersion seems to indicate that the Hα *EW* also varies at scales shorter than one year. Due to the heterogenous origin of the data, we have done a further test to check whether the Hα *EW* is indeed variable using only data given in Table 2 (on-line), treated homogeneously, excluding those points that may be affected by atmospheric lines, concretely those obtained with CARELEC at OHP, and the two much earlier 1992 and 1993 points. The resulting mean is -2.62 ± 0.01 Å with a standard deviation of 0.26, being also this data subset incompatible with a constant ($\chi^2_{\rm red}$ = 5.6, 24 d.o.f.). Although the strong dispersion of the data prevents us from making strong claims, it is worthy noting that the Hα *EW* seems to increase on average during the period 2003–2006, which would be evidence of a higher stellar mass-loss rate.

As noted in Sect. 1, a correlation between the Hα *EW* and the X-ray flux has been proposed in the past (e.g. R03; MS04) suggesting that larger stellar mass-loss rates are correlated with episodes of higher X-ray luminosity. These authors included in their comparison non-imaging 1998 *RXTE* data, and the X-ray observations used were taken at different orbital phases, being likely affected by additional orbital variability. Trying to avoid orbital variation effects and excluding *RXTE* data, we use *XMM-Newton* data taken in 2003 and 2005 around apastron and find that the flux in 2005 is only ≈10% larger (2σ level) than that observed in 2003. Otherwise, the Hα *EW* appears larger by ≈14% (6σ level; between -2.76 ± 0.05 Å to -2.43 ± 0.02 Å)[3], which could indicate variations of the stellar mass-loss rate by a factor of ∼2 (e.g., Puls et al. 1996, Table 7). Therefore, similar phase/epoch X-ray/Hα *EW* data point to a quite constant X-ray flux versus a significantly changing wind state. This absence of clear X-ray flux response to a significant change in the stellar mass-loss rate is at variance with the relation suggested by RO3 and MS04, although it is presently a two-points comparison.

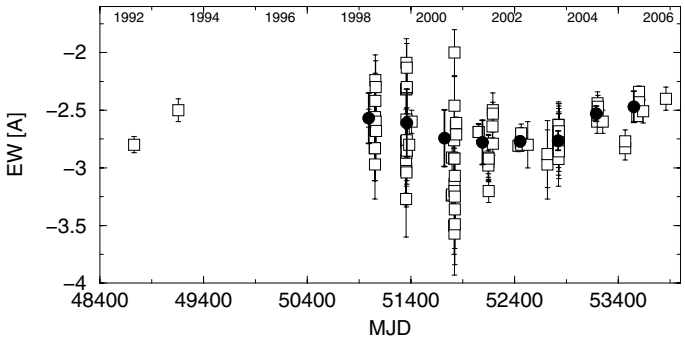

Fig. 3. The year averages (black circles) and the individuals points (white squares) for the Hα *EW*. For those years with several data points, the year average points are shown and their error bars represent the dispersion of values. The data come from this and previous works (C05: 2003; MS04: 1998, 1999, 2000, 2003; R03: 1999, 2002).

Finally, we show in Table 3 the 0.3–10 keV unabsorbed fluxes, photon indices and $N_{\rm H}$ (using the *wabs* model) values obtained by all instruments with imaging capabilities and working in the mentioned energy range. Using the values provided in that table, we obtain the following weighted mean values for the 0.3–10 keV flux, $(1.05 \pm 0.02) \times 10^{-11}$ erg cm^{-2} s^{-1} (fit-to-constant $\chi^2_{\rm red}$ = 8.4; 7 d.o.f.), the photon index, 1.54 ± 0.01 ($\chi^2_{\rm red}$ = 2.7; 7 d.o.f.), and $N_{\rm H}$, $(6.8 \pm 0.1) \times 10^{21}$ cm^{-2} ($\chi^2_{\rm red}$ = 0.7; 7 d.o.f.). Therefore, the flux found by all the instruments with imaging capabilities is clearly variable (dominated by orbital variability?) even when excluding the 2005 *Chandra* data point, the photon index seem to change as well with time, and the $N_{\rm H}$ is clearly compatible with being constant.

4.2. The N_H value and the location of the X-ray emitter

Photo-electric absorption in the dense wind of the primary in LS 5039 should increase the observed $N_{\rm H}$ to values above that due to the interstellar medium (ISM) alone. This effect could be detectable when comparing the values of the $N_{\rm H}$ inferred from X-ray and optical observations, respectively. However, the $N_{\rm H}$ values inferred from *XMM-Newton* data (using either *wabs* or *phabs*; see Sect. 2) are similar to, and somewhat smaller than, the value of the ISM $N_{\rm H}$ alone, which is $(7.3 \pm 1.1) \times 10^{21}$ cm^{-2}, derived using the $E_{\rm B-V}$ value from MS04 and the ISM $N_{\rm H}$-$E_{\rm B-V}$

[3] These has been obtained averaging few months data around the *XMM-Newton* observation dates, which implies to assume a steady Hα behavior at these timescales.

Table 3. Summary of the results for all the X-ray observations on LS 5039 performed by instruments with imaging capabilities. The unabsorbed fluxes in the energy range 0.3–10 keV, photon indices, and $N_{\rm H}$ (with *wabs* model) values are given. *BeppoSAX* flux errors are the flux dispersion accounting for the count rate changes by a factor of two during the observation and neglecting photon index variations. *ASCA* flux errors are assumed to be 10% of the flux. The given 2005 *XMM-Newton* $N_{\rm H}$ values are computed with the *wabs* model for comparison with 2003 values. For more details, see M05 (2003 *XMM-Newton* data), R03 (*BeppoSAX* data), and Yamaoka, K., private communication (*ASCA* data).

Date yyyy-MM-dd	MJD	Mission	Phase range	Flux (0.3–10 keV) $\times10^{-11}$ erg cm^{-2} s^{-1}	Photon index	$N_{\rm H}$ (*wabs*) $\times10^{21}$ cm^{-2}
1999-10-04	51 455.9	*ASCA*	0.38–0.47	0.80 ± 0.08	1.6 ± 0.1	7 ± 1
2000-10-01	51 818.5	*BeppoSAX*	0.97–0.21	0.5 ± 0.2	1.8 ± 0.2	10^{+3}_{-4}
2002-09-10	52 527.3	*Chandra*	0.71–0.73	0.8 ± 0.3	1.1 ± 0.2	6 ± 2
2003-03-08	52 706.3	*XMM-Newton*	0.54–0.57	1.03 ± 0.07	$1.56^{+0.02}_{-0.05}$	$7.2^{+0.3}_{-0.5}$
2003-03-27	52 725.8	*XMM-Newton*	0.55–0.58	0.97 ± 0.07	$1.49^{+0.05}_{-0.04}$	$6.9^{+0.5}_{-0.3}$
2005-04-13	53 473.1	*Chandra*	0.86–0.87	2 ± 1	1.1 ± 0.2	6±1
2005-09-22	53 635.8	*XMM-Newton*	0.49–0.53	$1.18^{+0.03}_{-0.07}$	1.51 ± 0.02	6.7 ± 0.2
2005-09-24	53 637.8	*XMM-Newton*	0.02–0.05	0.74 ± 0.07	1.59 ± 0.03	6.6 ± 0.2

relationship given by Predehl & Schmitt (1995)[4]. Taking into account the optical and *XMM-Newton* $N_{\rm H}$ values and error bars, we derive lower- and upper-limits of $\approx4.1\times10^{21}$ and 6.7×10^{21} cm^{-2} for the interstellar and total $N_{\rm H}$, respectively. This yields an upper-limit for the intrinsic $N_{\rm H}$ of $\approx2.6\times10^{21}$ cm^{-2}. In addition, the *XMM-Newton* $N_{\rm H}$ values around phases 0.5 and 0.0 are compatible with being constant, unlike what may be expected given the orbital eccentricity and inclination of the system (Sect. 1), which should introduce orbital variations in the $N_{\rm H}$ intrinsic to the wind. The 3σ-error of the difference of $N_{\rm H}$ between apastron and periastron is $\approx10^{21}$ cm^{-2}, which we adopt as an upper-limit to the intrinsic $N_{\rm H}$ variation between these two orbital phases.

To quantify whether the contribution of the stellar wind to the total $N_{\rm H}$ depends on the X-ray source location, we modeled the wind as spherically symmetric. We neglected X-ray irradiation effects since the modest X-ray luminosity of the source ($\lesssim10^{34}$ erg s^{-1}) is unlikely to ionize a large fraction of the wind, which could reduce the intrinsic $N_{\rm H}$ value. We estimate the distance at which X-rays would strongly ionize the wind to be $\lesssim1/10$ the orbital one (e.g., Blondin 1994). MS04 obtained similar constraints on the ionized wind region size. The radial wind velocity at a distance r from the star has been assumed to follow the law: $V_{\rm w} = V_\infty(1 - R_*/r)^\beta$, where $V_\infty = 2440$ km s^{-1} is the radial velocity of the wind in infinity, $\beta = 0.8$ is the wind profile exponent, $R_* = 9.3\ R_\odot$ is the stellar radius and r is the distance to the star (MS04; C05). The stellar mass-loss rate is taken to be in the range $\dot{M}_{\rm w} \sim 3.7$–$7.5\times10^{-7}\ M_\odot$ yr^{-1} (C05), which allows us to compute the wind density: $\rho_{\rm w} = \dot{M}_{\rm w}/4\pi r^2 V_{\rm w}$.

Integrating the wind density from the compact object location along the observer line of sight up to distances where the wind influence is negligible, we obtain an intrinsic $N_{\rm H}$ in the ranges $\sim$8–29×10^{21} and $\sim$2–5×10^{21} cm^{-2} around phases 0.0 and 0.5, respectively. To look for these minimum and maximum values of the wind $N_{\rm H}$, we adopted the most extreme values for the inclination and $\dot{M}_{\rm w}$. The wide range of possible values comes from the factor of 2 difference in the mass-loss rate and from the two extreme inclination angles. The $N_{\rm H}$ difference between the two orbital locations is expected to be in the range $\sim$3–27×10^{21} cm^{-2}, taking for this comparison the two extreme $\dot{M}_{\rm w}$ values, due to possible orbital variability, but the same i (that rendering either the smallest or the largest $N_{\rm H}$ difference). The wide range of N_H values is mainly explained by the fact that the line of sight can cross very different density regions at apastron and periastron passage depending on i.

The observed $N_{\rm H}$ seems fairly low taking into account the absorption from the ISM plus the intrinsic component we computed. At periastron passage, the intrinsic expected $N_{\rm H}$ value is 3 to 12 times larger than the stated upper-limit for this component. At apastron, the expected intrinsic $N_{\rm H}$ value is similar to its upper-limit. Stronger disparities are found when comparing the calculated intrinsic $N_{\rm H}$ variation between phases 0.5 and 0.0: a factor between 3 and 27 times larger than the upper-limit. It is worth noting that a similar wind model seems to work when applied, for instance, to the orbital $N_{\rm H}$ variation in 4U 1538−52 (Mukherjee et al. 2007), an X-ray binary system that presents X-ray absorption conditions along the orbit similar to those of LS 5039.

There are some cases in the literature about winds in massive isolated stars that appear to be less dense than expected (e.g. Kramer et al. 2003; Cohen et al. 2006). In these cases, wind clumping has been invoked to explain the low densities of the hydrogen column density inferred from X-ray observations, although a very special wind structure would be required to prevent the observed constancy of the $N_{\rm H}$ for such different orbital phases in LS 5039 if the emitter is well inside the system[5]. Real mass-loss rates much lower than those inferred from optical observations may be also a possibility. Another reason for this low intrinsic and/or constant $N_{\rm H}$ could be that X-rays are emitted where the stellar wind is already diluted. In particular, an emitter located along the line of sight should be beyond one orbital radius, $\approx2\times10^{12}$ cm, away from the compact object to explain the constancy of the $N_{\rm H}$ or its low intrinsic value. Different orientations of the system/emitter/observer geometry give similar constraints, thus we adopt $\sim10^{12}$ cm as a lower-limit for the emitter-compact object distance. Finally, to reduce the inferred $N_{\rm H}$, the X-ray emitter may be as large as the whole system, although in such a case the stellar wind would probably be affected to a much larger extent than it seems to be (e.g. via ionization).

4.3. The non-thermal emitter

The unabsorbed X-ray spectrum of LS 5039 is well explained by a pure power-law pointing to a non-thermal origin, and the data at higher energies obtained by *INTEGRAL* (De Rosa et al. 2006) show no hints of cutoff up to 100 keV, unlike what would be expected in a thermal comptonization scenario. Location of

[4] To obtain a conservative error for the $N_{\rm H} - A_{\rm V}$ relationship given in Predehl & Schmitt (1995), we use the dispersion and not the error of the mean.

[5] Such special wind structure may be produced by the slow compact object motion through the wind, although it can hardly have strong impact since the supersonic wind will efficiently convect outwards any possible perturbation.

the X-ray source at $\gtrsim 10^{12}$ cm from the compact object would also support a non-thermal nature for the high energy emission. Plausible mechanisms that could produce the keV–MeV spectrum could be synchrotron or inverse Compton processes, although solving this question is out of the scope of this work. We note that the lack of thermal features in the X-ray spectrum has been the main argument against accretion as the powering source in LS 5039, and a young non-accreting pulsar, producing the high energy emission via stellar/pulsar wind collision, has been proposed as the non-thermal emitter (e.g., M05; Dubus 2006).

The emission at TeV energies in LS 5039 is unlikely to be produced well inside the system since photon-photon absorption does not seem to be the only effect modulating the TeV emission (Aharonian et al. 2006). In addition, the optically thin nature of the radio emission at least down to ∼1 GHz (Martí et al. 1998), and the relatively small radio variability of the core ($\lesssim$50%), preclude a too compact radio emitter. We note that all this fits well in a scenario in which the X-ray emitter is at some distance from the compact object. Extended radio emission has been imaged in the range ∼1–100 mas, showing an approximately steady orientation of ±15° at different epochs and spatial scales as well as strong collimation (Paredes et al. 2000, 2002). It seems reasonable to associate such extended radio structure with the multiwavelength emitter. Whether this jet-like structure is powered by a different accretion mechanism, irrespective of its radiative properties, or it can be explained in the context of a more general young non-accreting pulsar scenario, remains an open question. In any case, understanding the complex radio, X-ray and TeV spectra and lightcurves, and the unclear X-ray-stellar wind link, requires further and accurate data plus modeling.

5. Summary

The 2005 *XMM-Newton* observations of LS 5039 presented here were carried out around apastron and periastron passages during an epoch of enhanced stellar mass-loss rate. The fluxes, photon indices, and $N_{\rm H}$ are $(1.18^{+0.03}_{-0.07})$ and $(0.74 \pm 0.07) \times 10^{-11}$ erg cm^{-2} s^{-1}, 1.51 ± 0.02 and 1.59 ± 0.03, and (6.3 ± 0.1) and $(6.2 \pm 0.2) \times 10^{21}$ cm^{-2}, at orbital phases ≈0.5 and 0.0, respectively. The reanalysis of 2005 *Chandra* observations yields a flux of $(2 \pm 1) \times 10^{-11}$ erg cm^{-2} s^{-1}, a photon index of 1.1 ± 0.2, and $N_{\rm H} = (6.2 \pm 0.2) \times 10^{21}$ cm^{-2}. The *XMM-Newton* fluxes and photon indices show variability (more marginal for the latter), whereas the $N_{\rm H}$ is compatible with being constant. *Chandra* data point to a hard spectrum, and possible higher fluxes, although the impact of pileup adds uncertainty to these results. Hα *EW* data collected since 1992 show that this quantity varies on timescales longer, and perhaps also shorter, than one year. Comparison of the Hα *EW* at the epochs when 2003 and 2005 *XMM-Newton* fluxes are available (at similar orbital phases), point to a quite constant X-ray flux versus significant Hα *EW* variations. If confirmed, this would disfavor a wind accretion scenario to explain the X-ray emission in the source. The constancy of the $N_{\rm H}$ points either to an emitter located at $\gtrsim 10^{12}$ cm from the compact object or to a stellar wind density between 3 and 27 times lower than those expected from a spherically symmetric stellar wind model, since ionization does not seem to affect significantly the wind absorption. An upper-limit on the intrinsic $N_{\rm H}$ is also derived, being between 3 and 12 times smaller than that predicted by the mentioned stellar wind model at periastron passage. We propose that the multiwavelength emitter is not located inside the binary system, probably being the jet-like structure observed at radio frequencies. In any case, simultaneous X-ray/optical observations are still required to clarify the stellar wind/X-ray link, and further *XMM-Newton* or *Chandra* X-ray observations are also necessary to further investigate the flux, photon index and intrinsic $N_{\rm H}$ evolution along the orbit.

Acknowledgements. We are grateful to M. V. McSwain for providing us with Hα *EW* information obtained during 1998, 1999, 2000 and 2003. We thank Dieter Horns and Jennifer R. West for fruitful discussions concerning the analysis of the *Chandra* data presented here. We thank Patrick Guillout, Olivier Herent, Rodrigo P. Campos, M. V. F. Copetti, Laerte Andrade, Adriana Mancini-Pires and Monica M. M. Uchida for conducting part of the optical observations at various observatories. V. B.-R. thanks the Max-Planck-Institut für Kernphysik for its support and kind hospitality. V. B.-R. gratefully acknowledges support from the Alexander von Humboldt Foundation. M.R. is being supported by a Juan de la Cierva fellowship from the Spanish Ministerio de Educación y Ciencia (MEC). V. B.-R., M.R. and J.M.P acknowledge support by DGI of MEC under grant AYA2004-07171-C02-01, as well as partial support by the European Regional Development Fund (ERDF/FEDER). I.N. acknowledges support by DGI of MEC under grant AYA2005-00095. R.L.O. acknowledges financial support from the Brazilian agency FAPESP (grant 03/06861-6). This work is based on observations obtained with XMM-*Newton*, an ESA science mission with instruments and contributions directly funded by ESA Member States and NASA.

References

Aharonian, F., Akhperjanian, A. G., Aye, K. M., et al. 2005, Science, 309, 746
Aharonian, F., Akhperjanian, A. G., Bazer-Bachi, A. R., et al. 2006, A&A, 460, 743
Balucinska-Church, M., & McCammon, D. 1992, ApJ, 400, 699
Blondin, J. M. 1994, ApJ, 435, 756
Bosch-Ramon, V., Paredes, J. M., Ribó, M., et al. 2005, ApJ, 628, 388 (BR05)
Casares, J., Ribó, M., Ribas, I., et al. 2005, MNRAS, 364, 899 (C05)
Cohen, D. H., Leutenegger, M. A., Grizzard, K. T., et al. 2006, MNRAS, 368, 1905
Davis, J. E. 2001, ApJ, 562, 575
De Rosa, A., Ubertini, P., Bazzano, A., et al. 2006, AdSpR, Proceedings from COSPAR 2006, ed. J. Vink, & P. Ghavamian, in press [arXiv:astro-ph/0611114]
Dubus, G. 2006, A&A, 456, 801
Goldoni, P., Ribó, M., Di Salvo, T., et al. 2006, Ap&SS, 309, 293
Hinkle, K. H., Wallace, L., & Livingston, W. 2003, BAAS, 35, 1260
Horns, D. for the HESS collaboration, 2nd Workshop On TeV Particle Astrophysics, Madison, August 2006
Kaufer, A., Stahl, O., Tubbesing, S., et al. 1999, The Messenger, 95, 8
Kramer, R. H., Cohen, D. H., & Owocki, S. P. 2003, ApJ, 592, 532
Lemaitre, G., Kohler, D., Lacroix, D., Meunier, J. P., & Vin, A. 1990, A&A, 228, 546
Martí, J., Paredes, J. M., & Ribó, M. 1998, A&A, 338, L71
Martocchia, A., Motch, C., & Negueruela, I. 2005, A&A, 430, 245 (M05)
McSwain, M. V., & Gies, D. R. 2002, ApJ, 568, L27
McSwain, M. V., Gies, D. R., Huang, W., et al. 2004, ApJ, 600, 927 (MS04)
Motch, C., Haberl, F., Dennerl, K., Pakull, M., & Janot-Pacheco, E. 1997, A&A, 323, 853
Mukherjee, U., Raichur, H., Paul, B., Naik, S., & Bhatt, N. 2007 [arXiv:astro-ph/0702142]
Paredes, J. M., Martí, J., Ribó, M., & Massi, M. 2000, Science, 288, 2340
Paredes, J. M., Ribó, M., Ros, E., Martí, J., & Massi, M. 2002, A&A, 393, L99
Predehl, P., & Schmitt, J. H. M. M. 1995, A&A, 293, 889
Puls, J., Kudritzki, R. P., Herrero, A., et al. 1996, A&A, 305, 171
Reig, P., Ribó, M., Paredes, J. M., & Martí, J. 2003, A&A, 405, 285 (R05)
Ribó, M., Reig, P., Martí, J., & Paredes, J. M. 1999, A&A, 347, 518

Online Material

Table 2. Hα *EW* measurements obtained from 1992 to 2006*.

Date (yyyy-MM-dd)	MJD	Orb. phase	Observatory	Instrument	Resolution	Setting**	Hα *EW* (Å)	Error (Å)
1992-04-19	48 731.250	0.85	ESO-2.20	EFOSC2	3000	–	−2.80	0.07
1993-06-19	49 257.010	0.45	OHP-193	CARELEC	450*	–	−2.50	0.10
1999-08-18	51 408.842	0.35	OAB	BFOSC	1600	Grism#7	−2.60	0.10
2000-09-08	51 795.813	0.42	OHP-193	ELODIE	45 000	–	−3.24	0.10
2000-09-10	51 797.768	0.92	OHP-193	ELODIE	45 000	–	−2.91	0.15
2000-09-12	51 799.768	0.43	OHP-193	ELODIE	45 000	–	−3.23	0.15
2000-10-18	51 835.984	0.70	ESO-1.52	FEROS	48,000	–	−2.64	0.05
2000-10-19	51 836.983	0.96	ESO-1.52	FEROS	48,000	–	−2.61	0.05
2000-10-20	51 838.000	0.22	ESO-1.52	FEROS	48,000	–	−2.71	0.05
2001-05-24	52 053.424	0.37	ESO-VLT-U1	FORS1	990	GRIS_600V	−2.69	0.07
2001-05-26	52 055.417	0.88	ESO-VLT-U1	FORS1	990	GRIS_600V	−2.69	0.07
2001-08-25	52 146.858	0.29	OHP-193	ELODIE	45 000	–	−2.95	0.10
2001-08-26	52 147.857	0.55	OHP-193	ELODIE	45 000	–	−2.98	0.10
2001-08-28	52 149.848	0.06	OHP-193	ELODIE	45 000	–	−2.91	0.20
2001-08-30	52 151.822	0.56	OHP-193	ELODIE	45 000	–	−2.92	0.20
2001-10-06	52 188.978	0.08	ESO-1.52	FEROS	48 000	–	−2.64	0.10
2001-10-07	52 189.992	0.33	ESO-1.52	FEROS	48 000	–	−2.79	0.10
2001-10-08	52 191.050	0.60	ESO-1.52	FEROS	48 000	–	−2.50	0.15
2001-10-09	52 192.000	0.85	ESO-1.52	FEROS	48 000	–	−2.53	0.10
2002-06-14	52 439.340	0.17	ESO-NTT	EMMI	5000	–	−2.81	0.05
2002-07-08	52 463.335	0.31	ESO-NTT	EMMI	5000	–	−2.78	0.05
2002-07-09	52 464.141	0.52	ESO-NTT	EMMI	5000	–	−2.80	0.05
2002-07-10	52 465.052	0.75	ESO-NTT	EMMI	5000	–	−2.72	0.10
2002-07-11	52 466.214	0.06	ESO-NTT	EMMI	5000	–	−2.70	0.05
2004-07-13	53 199.923	0.89	OHP-193	CARELEC	900*	Grating 133/375	−2.60	0.10
2004-07-14	53 200.937	0.15	OHP-193	CARELEC	900*	Grating 133/375	−2.54	0.10
2004-07-16	53 202.936	0.66	OHP-193	CARELEC	900*	Grating 133/375	−2.44	0.10
2004-07-18	53204.906	0.17	OAB	BFOSC	2000	Grism#8	−2.47	0.10
2004-09-02	53 250.935	0.95	LNA-0.60	ESPCASS	1460	–	−2.60	0.10
2005-04-07	53 467.299	0.34	LNA-1.60	ESPCASS	3,600	Grating 1200/750	−2.83	0.10
2005-04-07	53 467.299	0.34	LNA-1.60	ESPCASS	3,600	Grating 1200/750	−2.77	0.10
2005-07-31	53 583.748	0.16	ESO-NTT	EMMI	1100	Grism#5	−2.55	0.05
2005-08-20	53 602.935	0.07	LNA-1.60	ESPCASS	2,500	Grating 900/550	−2.39	0.05
2005-08-20	53 602.963	0.08	LNA-1.60	ESPCASS	2,500	Grating 900/550	−2.34	0.05
2005-08-21	53 603.078	0.10	LNA-1.60	ESPCASS	2,500	Grating 900/550	−2.43	0.05
2005-09-30	53 643.005	0.33	LNA-1.60	ESPCASS	730	Grating 300/640	−2.51	0.10
2006-05-07	53 862.181	0.44	NOT	ALFOSC	3000	Grism#16	−2.40	0.10

* Spectra with *EW* values corrected for the presence of blended telluric lines. ** The setting of the instrument is shown when relevant.